High-resolution and high-intensity powder diffractometer at BL15XU in SPring-8

Takuji Ikeda,[a]*† Atsushi Nisawa,[b] Masato Okui,[b] Nobuhiro Yagi,[b] Hideki Yoshikawa[b] and Sei Fukushima[b]

[a]Advanced Materials Laboratory, National Institute for Material Science, Namiki 1-1, Tsukuba, Ibaraki 305-0044, Japan, and [b]Harima Office, Advanced Materials Laboratory, National Institute for Material Science, Kouto, Mikazuki, Sayo, Hyougo 679-2148, Japan. E-mail: takuji-ikeda@aist.go.jp

A new ultra-high-resolution powder diffractometer for synchrotron radiation has been constructed at beamline BL15XU, SPring-8. The two-axis diffractometer is optimized for high-flux and high-coherent X-ray beams, which are provided by combining a planar undulator and a large offset rotated-inclined Si(111) double-crystal monochromator. The optics design of the diffractometer is based on transmission geometry, which employs a capillary specimen and reflection geometries using a flat-plate specimen. The intensity data are collected using a 2θ step-scan technique in both geometries. The diffractometer can be arranged in a variety of optical configurations, *e.g.* simple receiving slits, flat crystal analyzer of Ge(111) or Si(111), and in-vacuum-type long horizontal parallel slits. A minimum full width at half-maximum against 2θ was 0.00572° at λ = 0.63582 Å for the (200) reflections from Si powder in the transmission geometry employing the Ge(111) crystal analyzer. A wide temperature range (32–900 K), which is controlled by a He/N_2 gas stream system, is available. 288 structure parameters of a zeolite ZSM-5 sample have been demonstrated to successfully refine with a R_{wp} value of 6.96% by a Rietveld analysis of the high-resolution powder diffraction data from a 1 mm-diameter capillary specimen.

Keywords: powder diffraction; undulators; large-gap monochromators; zeolites.

1. Introduction

In material science a key to elucidating the origin of the physical and chemical properties is to determine the crystal structure. Numerous categories of functional materials, such as small organic molecules, zeolites and fullerene compounds, however, are obtained in polycrystalline forms. High-resolution synchrotron powder diffraction is a powerful tool for probing the crystal structures of these polycrystals. Parallel-beam optics using synchrotron radiation provides an angular resolution of 0.01–0.03° at the full width at half-maximum (FWHM) of the instrumental function. Various types of high-resolution powder diffractometers are commonly used, *e.g.* BM16 (Fitch, 1996) and SNBL at the ESRF, X3B1 and X7A at NSLS, BL-4B2 at KEK-PF (Toraya *et al.*, 1996), BL02B2 at SPring-8 (Nishibori *et al.*, 2001) and Station 2.3 at CLRC (Collins *et al.*, 1992).

The angle-dispersive transmission mode, also called the Debye–Scherrer geometry (Barnea *et al.*, 1992), is commonly adopted in modern high-resolution powder diffractometric systems. Since the trend in powder diffractometry is to use high-brilliance and high-energy light sources, the Debye–Scherrer geometry is more advantageous than the conventional reflection-mode geometry. In the Debye–Scherrer geometry, the sample is packed into a capillary glass tube. Some of the advantages are that the preferred orientation is reduced, a small volume is used and air-sensitive samples can be evaluated (Evain *et al.*, 1993). Limitations include a relatively high background level due to the capillary glass tube, samples with heavy metals that absorb X-rays, and relatively poor particle statistics owing to small sample volume.

A traditional two-axis diffractometer with a single counter can be equipped with various optical devices. Typically, when a Si or Ge crystal analyzer is used, high instrumental resolution, less than 0.01° FWHM, can be achieved. The crystal analyzer can discriminate X-ray fluorescence from the sample, but the analyzer can contribute its own fluorescence at the *K* edge. Generally, the crystal analyzer reduces the observed diffraction beam intensity, which can cause a serious problem especially for small specimens measured using the Debye–Scherrer geometry. This problem leads to a long measurement time and/or poor counting statistics.

An undulator X-ray source provides high-intensity and high-coherence photon beams. An undulator X-ray source has a photon flux which is at least 10^3 times greater than that of a bending-magnet device. Combining an undulator X-ray source and crystal analyzer optics will balance the advantages of high resolution and high intensity in powder diffractometry.

We have developed an ultra-high-resolution powder diffraction system (UHRPD) at BL15XU, a contracted beamline of the National Institute for Materials Science (NIMS), at SPring-8 (Fukushima *et al.*, 1999). The aim of our diffraction system is to collect high-resolution and high-diffraction intensity data from crystal structures of functional materials with complicated atomic arrangements, such as zeolites.

In the present report, the performance of the UHRPD system is evaluated. The angular resolution, profile shape and intensity of diffraction have been examined by measuring Si and LaB_6. The results of the Rietveld analysis (Rietveld, 1969), which was applied to the diffraction data from zeolites LTL and ZSM-5, are also presented.

2. Instrumentation

2.1. Concept

Transmission geometry using parallel-beam optics is widely used to collect data in synchrotron powder diffractometry; compared with reflection geometry, transmission geometry decreases the preferred orientation. It is important to obtain high-resolution and high-intensity data in the transmission geometry. The symmetric profile shape of the Bragg reflections is indispensable for profile fitting to accurately estimate the integral intensities.

Axial divergence induces an umbrella effect that leads to the asymmetric profiles in the low 2θ region. The asymmetric shape causes an insufficient fit between the observed and calculated profiles, but several profile functions can improve the fit (Finger *et al.*, 1994). Simultaneously, axial divergence considerably degrades the angular resolution of low-angle reflections (Masson *et al.*, 2001). The degree of the asymmetry increases as the lattice constant increases. Furthermore, remarkable asymmetric profiles are observed in high-energy diffraction experiments since the Bragg angle shifts to a lower 2θ region and curvatures of the Debye–Scherrer rings increase as the wavelength shortens (Aranda *et al.*, 1998). This optical aberration depends mainly on two factors. One is the crystallinity of the sample and the other is the optical layout, which includes the slit, analyzer and incident-beam divergence.

† Present address: National Institute of Advanced Industrial Science and Technology, AIST Tohoku, Nigatake 4-2-1, Miyagino-ku, Sendai, Miyagi 983-8551, Japan.

 © 2003 International Union of Crystallography • Printed in Great Britain – all rights reserved

Parallel incident beams are important in avoiding the umbrella effect and the degradation of the resolution. An undulator X-ray source provides a very high photon flux, which is over 10^3 greater than that of a bending source and small divergence incident beam. Adding a long Soller slit mounted downstream from the specimen remarkably suppresses the horizontal divergence of diffracted beams, but the intensity is degraded.

Components of the diffractometer BL15XU are based on the multiple-detector system (MDS), which Toraya *et al.* (1996) have constructed, although our diffractometer is equipped with a single detector arm. Either a crystal analyzer or in-vacuum-type long horizontal parallel slits (Parrish *et al.*, 1986; Toraya *et al.*, 1995) can be selected. The former gives a high angular resolution and a good signal-to-noise ratio, but its Bragg reflection angles must be realigned at each wavelength (Cox *et al.*, 1986). The latter is advantageous for obtaining a higher diffracted intensity, although it has a moderate angular resolution, 0.03–0.05° FWHM over the 2θ region, and is roughly independent of the wavelength (Parrish & Hart, 1987). In addition, a simple optical geometry on the 2θ arm using a pair of receiving slits can be adopted. The angular resolution of the receiving slits optics depends on the distance between the sample and the detector, and the slit width. It is not necessary to realign the optical axis for parallel slits (Hart, 1991) and the receiving slits when the wavelength is changed, but the signal-to-noise ratios using these devices depend on the fluorescence of the sample and/or the energy resolution of the detectors.

Combining the crystal analyzer optics and the undulator source will provide second-generation structure analyses since a high angular resolution of the instrumental function and a high signal-to-noise ratio are essential for obtaining sufficient peak separation and accurate integral intensities. The benefit of our diffractometer is that it has an undulator device with high photon density and high coherency. Moreover, measurements can be conducted at low temperatures (down to 32 K) using a gas stream cooler system, and the low-temperature system equipped with the diffractometer can be used for capillary specimens.

2.2. Beamline layout for XRD measurements

Fig. 1 shows the schematic layout of the XRD experiment at BL15XU. The light source is a revolver-type undulator (Hara *et al.*, 2001). The planar phase covers an energy range of 4–20 keV for the XRD experiments. The large-offset rotated-inclined monochromator with Si 111 reflections is mounted 36.7 m from the light source.

Spatial screening of the exit beam from the large-offset rotated-inclined monochromator with four-blade slits (FBS1) allows the higher-order harmonics to be ignored (Nisawa *et al.*, 2003). Above 8 keV the third-order reflections are less than 10^{-5} of that of the first-order reflections when the aperture size of the front-end slits is fixed at 0.3 mm × 0.3 mm. Typically, at the sample the observed photon flux and the energy resolution, $\Delta E/E$, are $\sim 5 \times 10^{12}$ photons s^{-1} (100 mA)$^{-1}$ and $\sim 1 \times 10^{-4}$ at 8 keV, respectively. The effective center beam size is close to 1 (H) mm × 0.5 (V) mm, which is adequate compared with the inner diameter of a capillary tube from 0.3 to 1.0 mm. The four-blade slits (FBS2) upstream of the diffractometer can adjust the beam size, if necessary.

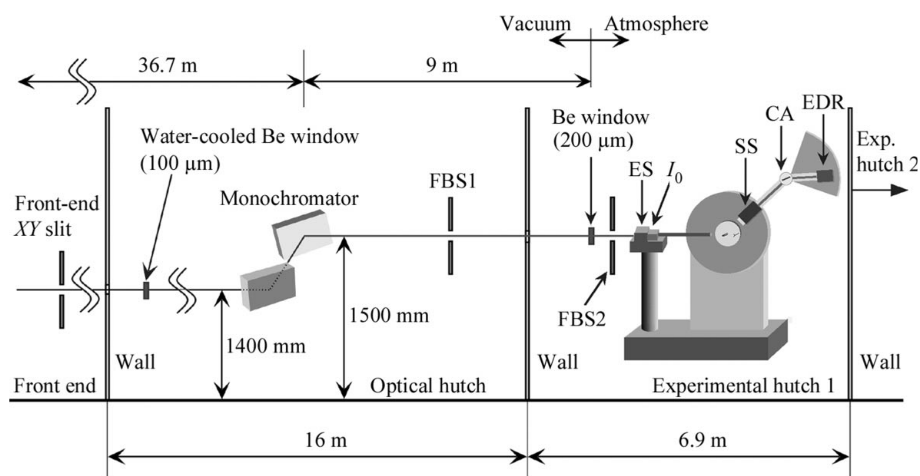

Figure 1
Schematic diagram of the powder diffraction experiment at BL15XU. FBS1 and FBS2: four-blade slits; ES: entrance stage; I_0: ion chamber as an incident beam monitor; SS: Soller slits; CA: crystal analyzer; EDR: enhanced dynamic range scintillation counter.

2.3. Goniometer system

Goniometer components and an electronic controller based on a SOR-PD1 synchrotron powder diffractometer were manufactured by Rigaku. This system is installed at $\sim$10 m from the monochromator (see Fig. 1). A single detector arm of length 690 mm is radially attached to the 2θ axis of the rotary table (Huber model 420 for θ axis and model 430 for 2θ axis). The rotation ranges of the θ and 2θ axes are $-3^\circ < \theta < 360^\circ$ and $-170^\circ < 2\theta < 170^\circ$, respectively, while that of the 2θ axis is limited by the analyzer devices on the detector arm. A Heidenhain encoder (PGM-246) reads the 2θ position with a minimum step of 0.0001°, the stepping motors can rotate the rotary table with the same step per pulse and the motor adjusts the height of the goniometer base to a beam height with a minimum step of 0.001 mm within its stroke from −15 mm to 5 mm. A rotary shutter, which has a through-hole of diameter 10 mm, and an ion chamber, I_0 beam monitor, are mounted on the entrance stage in front of the goniometer. The stepping-motor controller operates the horizontal and vertical positions of the entrance stage. A 625 mm vacuum path, which helps decrease the air scattering and the intensity loss of the diffracted beams, is mounted between the shutter box and the sample. Fig. 2 shows a photograph of the UHRPD equipped with the low-temperature system.

2.4. Analyzer, detector and sample stage

The detector arm is normally equipped with in-vacuum-type Soller slits (MacScience) with an angular aperture of 1°. A flat Ge(111) crystal analyzer stage is mounted at the end of the detector arm. An enhanced dynamic range scintillation counter (Bede EDR) with an yttrium–aluminium–phosphate scintillator and a normal NaI scintillation counter are also available. For the present beam size the evaluated count rate of the EDR detector was $\sim 2.4 \times 10^4$ counts s^{-1} within a linearity of 1% and $\sim 1.2 \times 10^5$ counts s^{-1} within a linearity of 5%. Correcting for the dead time, a count rate of $\sim 8 \times 10^5$ counts s^{-1} can be achieved within a linearity of 1%. The path length from sample position to scintillation counter is $\sim$920 mm. Two vacuum paths with lengths of 345 mm and 200 mm are mounted between the sample and the analyzer, and the analyzer and the

Table 1
Measurement conditions.

The wavelength λ, analyzer type and specimen are listed. RS indicates receiving slits optics with a width of 0.15 mm.

Sample	Si	Si	Si	LaB_6	LaB_6	ZSM-5	LTL
λ (Å)	0.63582	1.20001	1.54960	0.63585	0.63585	0.85001	1.20001
Capillary diameter (mm)	0.3	0.3	0.3	0.3	0.3	1.0	1.0
Analyzer type	Ge(111)	Ge(111)	RS	Ge(111)	RS	Ge(111)	Ge(111)
2θ range (°)	10–44.1	21–141	24–143	8.65–20.05	8–56	5–80	2–60
2θ step (°)	0.001	0.002	0.01	0.002	0.002	0.003	0.008

detector, respectively. Using the crystal analyzer configuration, rotation of the detector arm can measure a powder pattern over a 2θ range of 140°. Presently, in-vacuum-type long (400 mm) horizontal parallel slits with an angular resolution of 0.033° and a transmission coefficient of ∼42% (MacScience) can be used with the Soller slits, which have an overall aperture of about 10 mm × 10 mm.

Flat-plate powder experiments are also available. The sample is loaded onto a disk holder of diameter 30 mm and depth 0.5–1.0 mm. The disk usually rotates on a spinner mounted on the θ axis rotary table. The workstation can adjust the spinning rate and the height of the surface position. In the capillary mode, the flat-plat holder is replaced with a goniometer spinner. A telescope, which is mounted on a 2θ axis rotary table, can align the sample with the spin axis at the center of rotation. A DC motor maintains the spinning rate at a fixed speed of 60 r.p.m. The sample length should be about 15 mm and the minimum and maximum capillary diameters are 0.1 mm and 2.0 mm, respectively.

2.5. Low-temperature system

Low-temperature experiments in transmission geometry are carried out in a sample temperature range from 32 K to 300 K by using a gas stream cooler (CRYO Industries of America CRYO-COOL-CF3). He and N_2 gases from steel bottles and a nitrogen-gas generator, respectively, are cooled by two cold stages of the Gifford–McMahon-type closed-cycle refrigerator. A nozzle head, which is cooled by a top-to-bottom gas stream, is mounted above the sample. Two temperature controllers (Cryogenic Control Systems Model32 and Model34) with four sensors and three heaters accurately control temperatures at the sample, nozzle and cold stage positions. Normally, the gas flow rates are set at 13.5 L min^{-1} at 98 K using N_2 gas, and at 16 L min^{-1} at 32 K using He gas. To prevent air condensation on the surface of the capillary tubes and to adjust the gas streams between the nozzle and the sample, the capillary sample stage can be equipped with a detachable dry chamber (see Fig. 1). The dry chamber dramatically improves the stability of the sample temperature to within ±0.1 K.

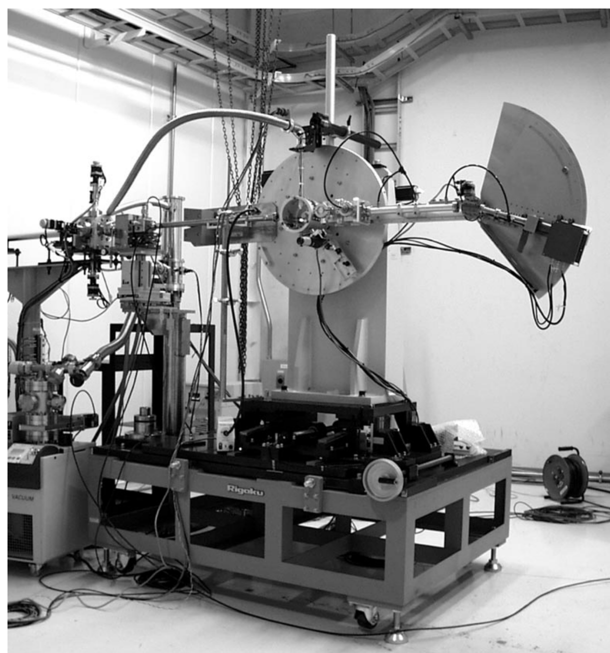

Figure 2
The diffractometer with a gas-flow-type low-temperature system inside experimental hutch 1 of the BL15XU at SPring-8.

2.6. Electronic component

A scaler–timer unit Canberra 2071A, a pulse motor driver and a standard-type high-voltage (HV) power supplier/pulse-height analyzer (PHA) were installed in a console rack. A workstation (Hewlett Packard E132L) controls the operation of the system, while the HV/PHA controller of the EDR detector and the temperature controllers are independently operated.

3. Experimental and data analysis

The performance of the UHRPD was evaluated at beamline BL15XU, SPring-8. The test samples were National Institute of Standards and Technology (NIST) Standard reference Material (SRM) 640c Si and 660 LaB_6, commercialized zeolite Linde Type L (LTL, $K_9Al_9Si_{27}O_{72}$, *P*6/*mmm*: TOSO HSZ-500KOA) and synthesized zeolite ZSM-5 ($Si_{96}O_{192}$, $P2_1/c$). The samples were loaded into a borosilicate glass capillary tube with an inner diameter of 0.3 mm for Si and LaB_6, and of 1.0 mm for ZSM-5 and LTL. To decrease the contribution of the preferred orientation, the capillary specimens are normally rotated. Table 1 lists the experimental conditions. The idle running time after each step scan was set to 0.8 s in order to decrease the vibrations of the 2θ arm while counting. Monochromatic X-ray beams with wavelengths of 0.63582, 0.85001, 1.20001 and 1.54960 Å were used in the measurements. A Ge(111) crystal analyzer or a pair of receiving slits with a width of 0.15 mm were used. Transmittance of direct incident beams determined the μr values (μ: linear absorption coefficient; r: sample radius) of the samples and capillary tubes, and the X-ray absorption was corrected. Intensity data were measured using scanning steps from 0.002 to 0.008° and a counting time of 1 s per step at room temperature.

The individual profile-fitting method using a multi-purpose pattern-fitting system, RIETAN-2000, initially analyzed the obtained intensity data for Si and LaB_6. Each profile was then fit to the modified split pseudo-Voigt function (Izumi & Ikeda, 2000) based on Toraya's split pseudo-Voigt function (Toraya, 1990). The *U*, *V* and *W* parameters in the Caglioti *et al.* (1958) formula for the FWHM were adopted. The background was approximated by a composite background function, *i.e.* 11th-order Legendre polynomial multiplied by a

set of numerical values. These numerical values for the preliminarily background were obtained using the computer program *Powder X* (Dong, 1999). The partial profile relaxation was applied to reflections with anisotropic broadening and/or a strongly asymmetric profile shape in the low 2θ region, which improved the fit between the observed and calculated profiles.

The intensity data of zeolite LTL and ZSM-5 were also analyzed by the Rietveld method utilizing RIETAN-2000. The coefficients for the analytical approximation of the atomic scattering factors for Si^{4+}, Al^{3+} and K^{+} were taken from *International Tables for X-ray Crystallography* (1974), and that for O^{2-} was given by Tokonami (1965). The program *CROMER* using the Cromer–Liberman method adopting the Kissel–Pratt correction evaluated the anomalous scattering factors (Kissel & Pratt, 1990).

4. Results and discussion

4.1. Evaluation of the angular resolution, profile shapes and intensity using Si and LaB_6 data

Figs. 3(*a*) and 3(*b*) show the results of the individual profile fittings for Si and LaB_6, respectively, at λ = 0.63582 Å. The estimated maximum angular resolution FWHM was 0.00572 (5)° for the Si (220) reflections and 0.00596 (8)° for the LaB_6 (200) reflections. The profile shapes for both reflections were ideally symmetric. The angular resolution of our diffractometer approaches that of the ultra-high-resolution powder X-ray diffractometer BM16 at the ESRF (Masson *et al.*, 2001).

Fig. 4(*a*) shows the 2θ dependence of FWHM values for Si, LaB_6 and zeolite samples for each wavelength and optical system. The calculated FWHM curves show a minimum value near $2\theta \simeq 20°$ because the optical aberration for the umbrella effect is not completely removed. A deviation of the FWHM value was observed for each FWHM curve, which indicates that the sharp instrumental function causes line-broadening effects from the crystallite size and strain (Cox, 1992). Fig. 4(*b*) shows the dependence of $\Delta d/d$ values on the lattice-plane spacing, *d*. The $\Delta d/d$ values given by FWHM (2θ) $\times$ cot θ are normally used to evaluate the peak separation (Czjzek *et al.*, 1992). The estimated $\Delta d/d$ values were smaller than $\sim$0.1% in the range 0.5 Å < *d* < 3.0 Å and the maximum resolution was $\Delta d/d \simeq$ 0.03%, which is comparable with the highest-resolution time-of-flight neutron powder diffractometer HRPD in ISIS (Ibberson *et al.*, 1992). The diffracted peaks were sharper at shorter wavelengths when employing the crystal analyzer. Thus, the overall $\Delta d/d$ resolution is roughly independent of the wavelength.

The observed profile shapes were almost symmetrical, but differed slightly for each optical configuration. The receiving optics with a pair of slits gave a Gaussian-type profile shape, represented by a window function based on the slit width. On the other hand, the Ge(111) crystal analyzer provided a radical profile shape with a long tail. In the tail of a strong reflection, a gradual small bump, which was due to the X-ray fluorescence scattering near the *K* edge of Ge, was observed at λ = 1.2 Å.

The diffracted intensity was $\sim 3.7 \times 10^4$ counts s^{-1} for Si (220) reflections and $\sim 6.2 \times 10^4$ counts s^{-1} for Si (111) reflections using only 0.1 mg of the sample. For the LaB_6 sample, the diffracted intensity was 9.6×10^4 counts s^{-1} for the (110) reflection at the peak maximum and 2.6×10^4 counts s^{-1} for the (200) reflection. Nevertheless, an Al attenuator, 700 µm thick, was inserted in front of the EDR detector.

4.2. Rietveld analysis of zeolites

Many structure studies of zeolite materials using synchrotron powder diffraction are reported. The counting statistics of their diffraction data, however, are usually insufficient (Eylem *et al.*, 1996) because of the low density and/or low crystallinity of zeolites. A powerful incident beam using an undulator source provides a good counting rate and saves measurement time in high-resolution powder diffraction.

Two other test samples of LTL and ZSM-5 have a complicated crystal structure, which include numerous atoms in a unit cell. In zeolites, a low density and small scattering amplitudes of the major chemical species such as Si, Al and O atoms result in a weak diffracted intensity. In their powder patterns, numerous reflections are overlapped without high peak separation.

The intensity data of zeolite LTL was measured over a 2θ range of 58° with a step interval of 0.008° at λ = 0.85001 Å. The measurement time was relatively short, about 3.6 h. Fig. 5 shows the results of the Rietveld analysis in zeolite LTL. For the 2θ region in Fig. 4, the angular resolution was moderate at 0.04–0.16° FWHM. A maximum

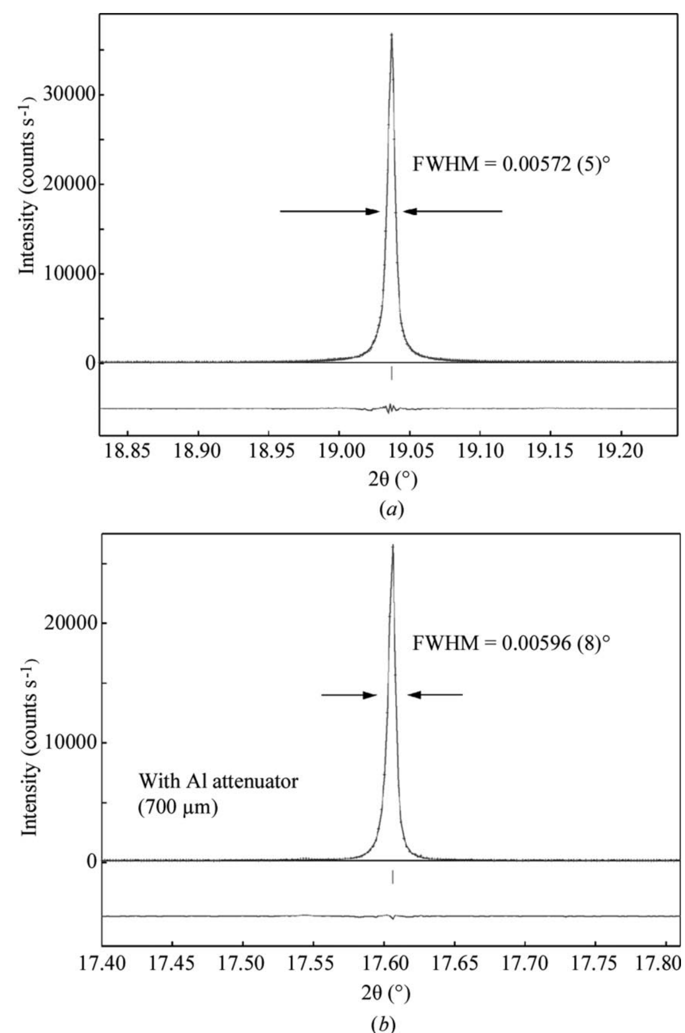

Figure 3
Individual profile fits for (*a*) the 220 reflections from Si and (*b*) the 200 reflections from LaB_6 in transmission mode at λ = 0.63582 Å. The cross-shaped points and the solid line represent the observed and calculated intensity, respectively. The difference plot is at the bottom of the pattern. A short vertical bar indicates the Bragg position.

peak intensity of $\sim$5.85 $\times$ 10^5 counts s^{-1} with a peak-to-background ratio of 300 was observed for 100 reflections at 2θ = 3.05°. The lattice parameters were a = 18.4659 (3) and c = 7.47739 (9) Å. The refined structural parameters of 12 independent sites were consistent with those described in a previous work (Barrer & Villiger, 1969). The R factors were quite low, R_{wp} = 4.90% (R_e = 1.98%), R_p = 3.19%, R_B = 1.60% and R_F = 1.59%, and the R_F value is much smaller than the value in previous work. For example, 13% (Barrer & Villiger, 1969) or 17% (Artioli & Kvick, 1990) were previously reported using powder diffraction data.

Fig. 6 shows the results of Rietveld analyses in ZSM-5. The wavelength and the step interval are 0.85001 Å and 0.003°, respectively. The whole powder pattern was recorded over a 2θ range of 75°, which covered 6923 Bragg reflections. The measurement time of 12.5 h was suitable for practical use considering the large number of scan steps (25 000). The lattice parameters were refined with a high degree of precision at a = 19.89701 (7), b = 20.12520 (5), c = 13.38005 (4) Å and β = 90.6167 (2)°. The starting model with 288 structure parameters of 72 independent sites (van Koningsveld *et al.*, 1990) was efficiently refined by the Rietveld analysis. The standard deviation of the refined structural parameters was sufficiently small and agreed with the results of a single-crystal experiment in Koningsveld's work.

The angular resolution of each reflection was extensively high with 0.013–0.052° FWHM (Fig. 4) in zeolites. The maximum peak intensity was $\sim$3.2 $\times$ 10^5 counts s^{-1}, but the background levels were lower than 260 counts s^{-1}. The peak-to-background ratio was 1230. For a large d-spacing region of d > 10 Å, $\Delta d/d$ was less than 0.06%. Partial profile relaxations (Ohta *et al.*, 1997) adopted for seven low-indexed reflections decreased the R factors: R_{wp} = 6.96% (R_e = 2.91%), R_p = 4.86%, R_B = 2.31% and R_F = 1.53%.

The data and profile shapes in the low 2θ region were less than 8° and were symmetric because the horizontal Soller slits effectively suppressed the axial divergence of the diffracted beams (Fig. 7). Table 2 lists the refined profile parameters: asymmetry As, dumping factors EtaL and EtaH.

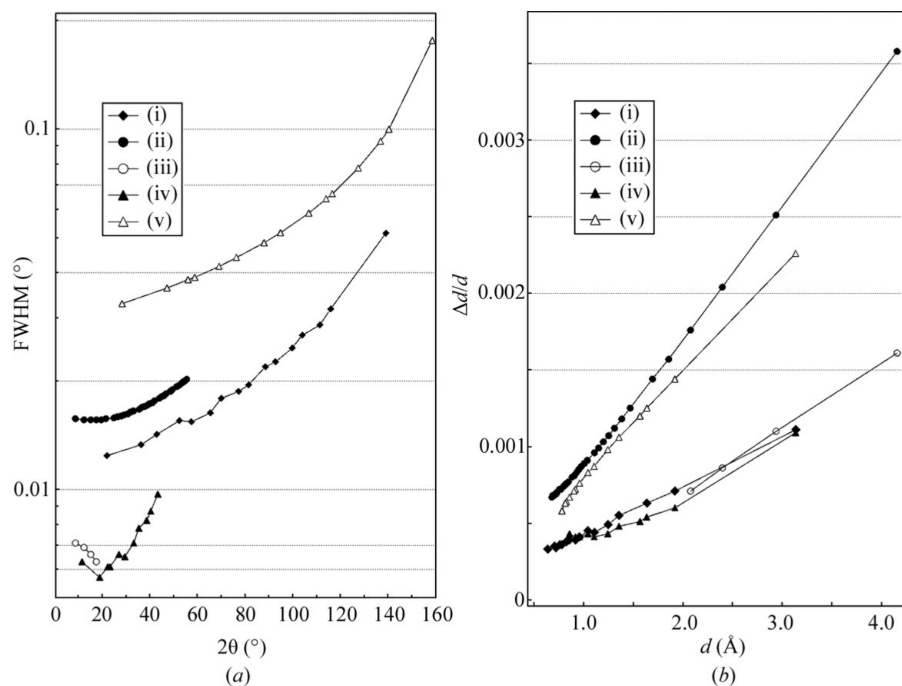

Figure 4
(a) The 2θ dependence of FWHM and (b) the d-spacing dependence of $\Delta d/d$ approximated by the individual profile fit. (i) Si measured at λ = 1.20001 Å using a Ge(111) analyzer, (ii) LaB_6 measured at λ = 0.63582 Å using receiving slits, (iii) LaB_6 measured at λ = 0.63582 Å using a Ge(111) analyzer, (iv) Si measured at λ = 0.63582 Å using a Ge(111) analyzer, (v) Si measured at λ = 1.54960 Å using receiving slits.

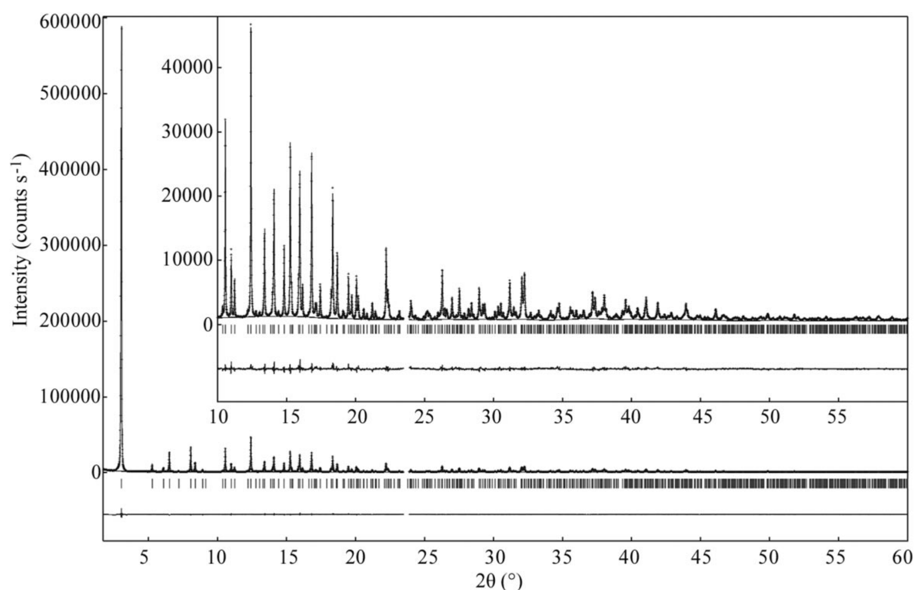

Figure 5
Results of the Rietveld refinement for the zeolite LTL sample. Observed, calculated and difference patterns for ZSM-5 are plotted against 2θ.

5. Conclusions

Measuring standard materials and zeolites demonstrated the versatility and ability of our powder diffractometer constructed at beamline BL15XU. An amazingly high angular resolution and high counting rates were achieved by combining the undulator X-ray source and the UHRPD equipped with crystal analyzer optics. In addition, the simple arrangement of the components from the undulator to the exit beam conveniently aligned the experimental set-ups by changing the wavelength.

The obtained data have prompted us to investigate structurally challenging materials. It is expected that the UHRPD will work well for *ab initio* structural determination, accurate electron density studies of zeolites (Ikeda *et al.*, 2002) and phosphate (Belik *et al.*, 2002), phase transitions with very weak super-lattice reflections, measuring a few

Table 2
Profile parameters As, EtaL and EtaH for low-angle reflections are listed after the Rietveld refinement of zeolite LTL and ZSM-5.

The parameters for the −101 and 011 reflections in ZSM-5 are constrained because two reflections are almost overlapped.

	LTL	ZSM-5					
	100	−101, 011	101	020	200	−111	002
As	2.36 (3)	2.34 (4)	1.82 (2)	2.46 (4)	1.93 (2)	1.84 (3)	1.51 (2)
EtaL	0.434 (4)	0.50 (2)	0.49 (2)	0.408 (6)	0.596 (8)	0.381 (14)	0.55 (2)
EtaH	0.957 (7)	0.94 (2)	0.95 (3)	0.91 (2)	0.924 (11)	0.69 (2)	0.73 (3)

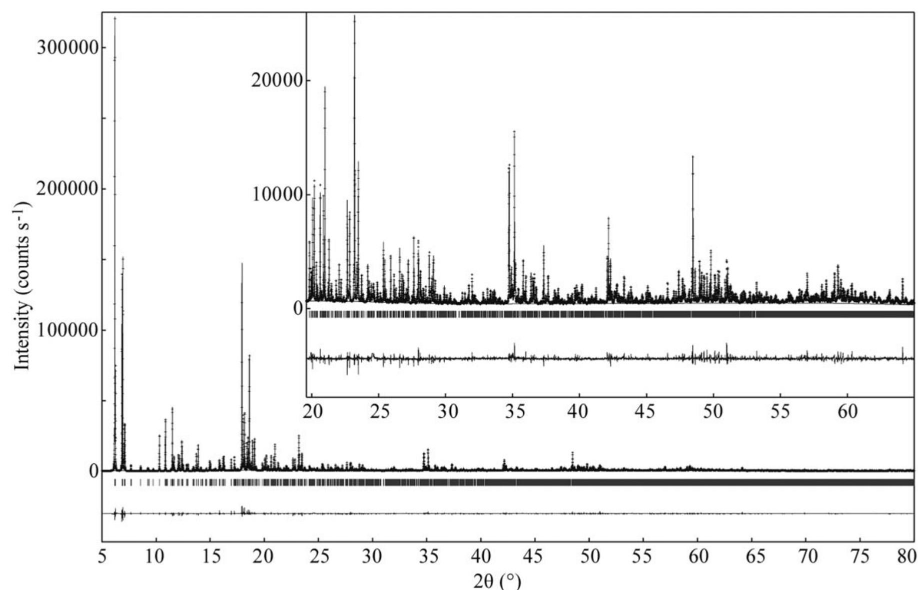

Figure 6
Results of the Rietveld refinement for the zeolite ZSM-5 sample.

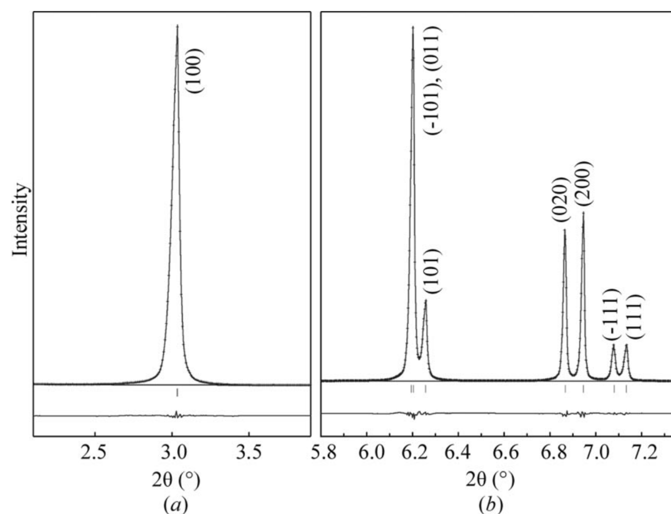

Figure 7
Profile shapes of the low 2θ regions for (*a*) LTL and (*b*) ZSM-5.

hundred nanogram samples, and so on. These structural studies are now in progress.

We thank F. Izumi for his help in data analyses and for fruitful discussion and comments, and Y. Kiyozumi for providing the ZSM-5 sample.

References

Aranda, M. A. G., Losilla, E. R., Cabeza, A. & Bruque, S. (1998). *J. Appl. Cryst.* **31**, 16–21.

Artioli, G. & Kvick, Å. (1990). *Eur. J. Mineral.* **2**, 749–759.

Barnea, Z., Creagh, D. C., Davis, T. J., Garrett, R. F., Jansky, S., Stevenson, A. W. & Wilkins, S. W. (1992). *Rev. Sci. Instrum.* **3**, 223–228.

Barrer, R. M. & Villiger, H. (1969). *Z. Kristallogr.* **128**, 352–270.

Belik, A. A., Izumi, F., Ikeda, T., Morozov, V. A., Dilanian, R. A., Torii, S., Kopnin, E. M., Levedev, O. I., van Tendeloo, G. & Lazoryak, B. I. (2002). *Chem. Mater.* **14**, 4464–4472.

Caglioti, G., Paoletti, A. & Ricci, F. P. (1958). *Nucl. Instrum.* **3**, 223–228.

Collins, S. P., Cernik, R. J., Pattison, P., Bell, A. M. T. & Fitch, A. N. (1992). *Rev. Sci. Instrum.* **63**, 1013–1014.

Cox, D. E. (1992). *Synchrotron Radiation Crystallography*, pp. 186–254. New York: Academic Press.

Cox, D. E., Hastings, J. B., Cardoso, L. P. & Finger, L. W. (1986). *Mater. Sci. Forum*, **9**, 1–20.

Czjzek, M., Vogt, T. & Fuess, H. (1992). *Zeolites*, **12**, 237–239.

Dong, C. (1999). *J. Appl. Cryst.* **32**, 838.

Evain, M., Deniard, P., Jouanneaux, A. & Brec, R. (1993). *J. Appl. Cryst.* **26**, 563–569.

Eylem, C., Hriljac, J. A., Ramamurthy, V., Corbin, D. R. & Parize, J. B. (1996). *Chem. Mater.* **8**, 844–849.

Finger, L. W., Cox, D. E. & Jephcoat, A. P. (1994). *J. Appl. Cryst.* **27**, 892–1000.

Fitch, A. N. (1996). *Mater. Sci. Forum*, **228**/**231**, 219–222.

Fukushima, S., Yoshikawa, H. & Nisawa, A. (1999). *SPring-8 Annual Report*, pp. 97–99. SPring-8, Japan.

Hara, T., Tanaka, T., Sekine, T., Maréchal, X., Nisawa, A., Fukushima, S., Yoshikawa, H. & Kitamura, H. (2001). *Nucl. Instrum. Methods*, A**467**, 161–164.

Hart, M. (1991). *Mater. Sci. Forum*, **9**, 39–46.

Ibberson, R. M., David, W. I. F. & Knight, K. S. (1992). *The High Resolution Neutron Powder Diffractometer (HRDP) at ISIS – A User Guide*, Report RAL-92-031. Rutheford Appleton Laboratory, Oxon, UK.

Ikeda, T., Kodaira, T., Oh, T. & Nisawa, A. (2002). *Microporous Mesoporous Mater.* **57**, 249–261.

International Table for X-ray Crystallography (1974). Vol. C, 2nd ed., pp. 572–574. Dordrecht: Kluwer.

Izumi, F. & Ikeda, T. (2000). *Mater. Sci. Forum*, **321**/**324**, 198–203.

Kissel, L. & Pratt, R. H. (1990). *Acta Cryst.* A**46**, 170–175.

Koningsveld, H. van, Jansen, J. C. & van Bekkum, H. (1990). *Zeolites*, **10**, 235–242.

Masson, O., Dooryhee, E., Cheary, R. W. & Fitch, A. N. (2001). *Mater. Sci. Forum*, **378**/**381**, 300–305.

Nisawa, A., Okui, M., Yagi, N., Mizutani, T., Yoshikawa, H. & Fukushima, S. (2003). *Nucl. Instrum. Methods*, A**497**, 563–568.

Nishibori, E., Takata, M., Kato, K., Sakata, M., Kubota, Y., Aoyagi, S., Kuroiwa, Y., Yamakata, M. & Ikeda, N. (2001). *Nucl. Instrum. Methods*, A**467**/**468**, 1045–1048.

Ohta, T., Izumi, F., Oikawa, K. & Kamiyama, T. (1997). *Physica B*, **234**, 1093–1095.

Parrish, W. & Hart, M. (1987). *Z. Kristallogr.* **179**, 161–173.

Parrish, W., Hart, M., Erickson, C. G., Masciocchi, N. & Hung, T. C. (1986). *Adv. X-ray. Anal.* **29**, 243–250.

Rietveld, H. M. (1969). *J. Appl. Cryst.* **2**, 65–71.

Tokonami, M. (1965). *Acta Cryst* **9**, 486.

Toraya, H. (1990). *J. Appl. Cryst.* **23**, 485–491.

Toraya, H., Hibino, H. & Ohsumi, K. (1996). *J. Synchrotron Rad.* **3**, 75–83.

Toraya, H., Takata, M., Hibino, H., Yoshino, J. & Ohsumi, K. (1995). *J. Synchrotron Rad.* **2**, 143–147.

Received 2 August 2002 • Accepted 14 August 2003